HORIBA Scientific

20 YEARS 1819-2019 HORIBA JOBIN YVON

AFM-Raman

TERS Characterization of Graphene Nanoribbons

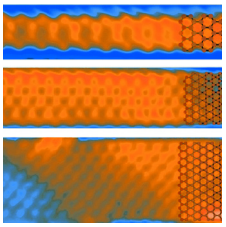

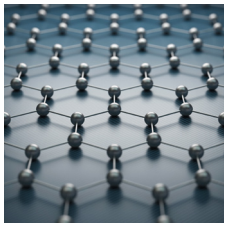

Application Note

Graphene/2D Materials AFM21

Ophélie Lancry, Agnès Tempez, Marc Chaigneau
HORIBA FRANCE SAS, Palaiseau, France.

Abstract : This application note reports on the TERS nanocharacterization of graphene nanoribbons (GNRs) fabricated by electron beam lithography. The chemical nanoresolution achievable by TERS reveals the presence of amorphous carbon at the edge of the GNRs and locates organic residues. TERS can be considered as a valuable tool for characterizing nanopatterned graphene, an essential step for the development of graphene-based nano-devices.

Keywords : Graphene, Nanoribbons, Nanopatterning, Tip-enhanced Raman spectroscopy.

Context and issues

No need to recall the exceptional properties of graphene which has driven tremendous research since Novoselov's scotch tape experiment[1-2]. Graphene is thus now foreseen for a handful of electronic and optoelectronic nano-devices[3]. Making nano-devices out of graphene requires nanopatterning. With a sub-10 nm resolution, electron beam lithography (EBL) is an option but it can generate defects and contamination[4-6]. As a result, determining the quality of patterned graphene is essential and detection of defects demands a sensitive chemical nano-characterization tool.

Potential/ Input from technique

Tip-Enhanced Raman Spectroscopy (TERS) has emerged as a powerful analytical technique providing high chemical sensitivity for surface molecular imaging with a nanoscale spatial resolution[7-10]. TERS enables characterization of nanopatterned graphene and reveals the presence of defects and impurities left by the resist, which could result in unwanted doping effect and lower carrier mobility.

Starting point, what is known?

TERS has been successfully used to characterize a variety of graphene properties such as number of layers, local strain, edge, surface adsorbates[10], and artificial defects.

Description of sample and measurement

Using natural graphite crystals and mechanical exfoliation method, monolayer graphene flakes were isolated on SiO_2(≈300 nm)/Si substrate. Then flakes have undergone the following process steps (schematically illustrated in Fig. 1) to produce graphene nanoribbons:

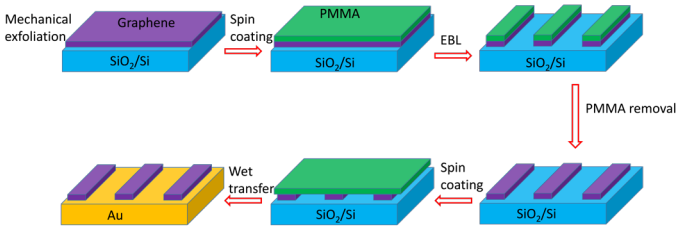

Fig. 1. Schematic diagram of fabrication steps of GNRs and their transfer from SiO_2/Si substrate to Au coated SiO_2/Si substrate.

- Electron resist (PMMA) deposition: spin coating and baking;
- EBL: beam exposition, development of exposed regions (in solvent), removal of non protected graphene using oxygen plasma. The protecting PMMA mask is then removed in acetone and the sample is dried: GNR with a width of about 60±5 nm, a length of >100 µm and an interdistance of 140 nm are created on SiO_2/Si substrate;
- Transfer of GNR on gold coated substrate by wet method: spin coating of 200 nm thick PMMA, baking, taping of frame (windowed on GNR region), KOH dipping to detach GNR from SiO_2/Si, application on a 100 nm Au coated substrate, PMMA removal, and annealing to reduce PMMA residues.

TERS measurements were performed in gap mode using a NanoRaman system from HORIBA Scientific integrating an atomic force microscope (OmegaScope, based on SmartSPM) and a Raman microscope (Labram Evo) with a 100× WD objective tilted by 60° with respect to the sample plane. A 638 nm *p*-polarized laser (130 µW) was focused onto the cantilever-based gold coated AFM-TERS tip (OMNI TERS-SNC-Au, App Nano). Transition between the pixels of the TEPL map is performed in alternating-contact mode, which preserves both the sharpness and plasmonic

enhancement of the tip eliminating lateral forces that might otherwise result in sweeping aside or picking up loosely attached contaminants from the sample surface.

First, AFM topography and phase images are measured to locate GNRs. As shown in Fig. 2a and 2b, GNRs are not clearly seen in the topography image due to the high roughness of the gold surface (RMS ≈1.0 nm) but a nice contrast in the phase image enables measurement of GNR width to be 57.2 ± 8.4 nm, which agrees well with the designed width of 60 nm.

Next, a TERS spectrum is collected in the interior of the GNRs. As shown in Fig. 2c, the spectrum features the G peak (~1585 cm^{-1}) corresponding to the E_{2g} phonon at the centre of the Brillouin zone and the 2D peak (~2637 cm^{-1}, overtone of the D peak) originating from scattering of the electron by two phonons having momentums q and -q [11]. The 2D peak is fit with single Gaussian peak with a width of 42 cm^{-1} which indicates the monolayer nature of the GNRs[11].

TERS mapping was conducted in the marked area of Fig. 2a and 2b, with scanning area of 600×300 nm^2 and a pixel size of 5 nm. The Raman intensity maps of the D, G and 2D modes are shown in Fig. 2d, 2e, and 2f, respectively upon fitting with three Lorentzian curves at ~1340, ~1585, and ~2637 cm^{-1}. TERS D peak intensity profile extracted from the line marked in Fig. 2d is shown in Fig. 2g to estimate the TERS spatial resolution. A fitted Gaussian peak exhibits a width of 5 ± 0.4 nm, which means, given the 5 nm pixel size, that resolution is limited by the sampling step and could be better than 5 nm (reported values as low as 1 nm for graphene [10,12-13] and graphene oxide [14]).

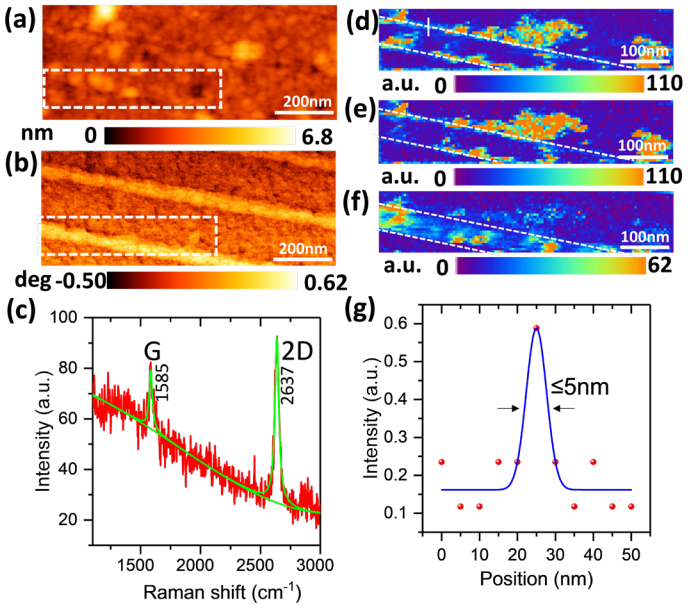

Fig. 2. AFM topography (a) and phase (b) images of GNRs ; (c) TERS spectrum measured in the GNR centre fitted by two Lorentzian functions; (d) D (e) G and (f) 2D TERS images of the GNR in marked regions of (a)-(b) 120×60 pixels, pixel size: 5 nm, exposure time: 0.7 s; (g) The typical spatial resolution obtained by fitting the line profile along the marked line in (c) using a Gaussian function.

Higher D and G signals are observed on the edge of the nanoribbon where 2D intensity is higher in the inner part. The D peak (~1340 cm^{-1}), which arises from the TO phonons around the K point of the Brillouin zone and requires scattering by a defect in order to maintain the conservation of momentum is an indication of the defect density. The EBL process splits the graphene flake into nanoribbons with large length/width ratio and induces the formation of high density of defects at the cutting interface, i.e. GNR edges[4]. A high D peak intensity is usually observed on the edges of mechanically exfoliated [11-12] or chemical vapor deposition grown graphene flakes. However, if one looks at spectra (1-5) taken on a line across the GNR edge from the substrate to the inner GNR (in the zoomed region in Fig. 3a), further information can be extracted. Spectra 2 and 3 taken on the GNR edge not only feature enhanced D and G peak signals but also no 2D peak.

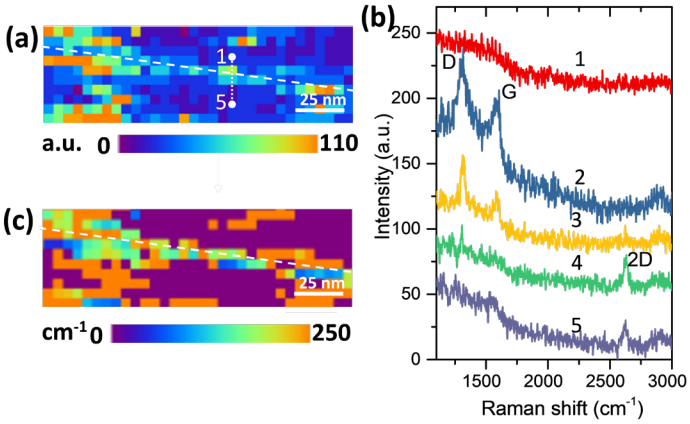

Fig. 3. TERS D peak intensity (a) and width (b) images of an area at the GNR edge in Figure 2(c); (c) Five TERS spectra along the marked line in (a).

Furthermore, the width of both D (width going from 38 to 86 cm^{-1}) and G (width going from 28 to 66 cm^{-1}) bands increases going from spectrum 3 to spectrum 2 whilst approaching the GNR edge. This is in contrast with what is observed at the edge of mechanically exfoliated monolayer graphene[12] and indicates the presence of a disordered graphene phase[15]. This implies that upon EBL, a band of damaged graphene (amorphous/disordered graphene) of a width of 5-10 nm is induced due to high energy electron bombardment.

The presence and local distribution of organic contamination have also been analyzed by plotting the 2890 cm^{-1} Raman band (stretching vibration C-CH_3) and upon fitting it with a single Lorentzian function. The TERS intensity image (Fig. 4a) indicates the presence of organic adsorbates on spots in both GNR and substrate areas. Four spectra are plotted in Fig. 4b on four locations featuring high intensity of the 2890 cm^{-1} Raman band: two in GNR area (P1-P2), two on the substrate(P3-P4). The presence of C-CH_3 signature indicates the presence of organic contaminants on the GNR samples, which most likely comes from the PMMA residues during the resist deposition process or/and the Si/SiO_2 to Au transfer substrate step.

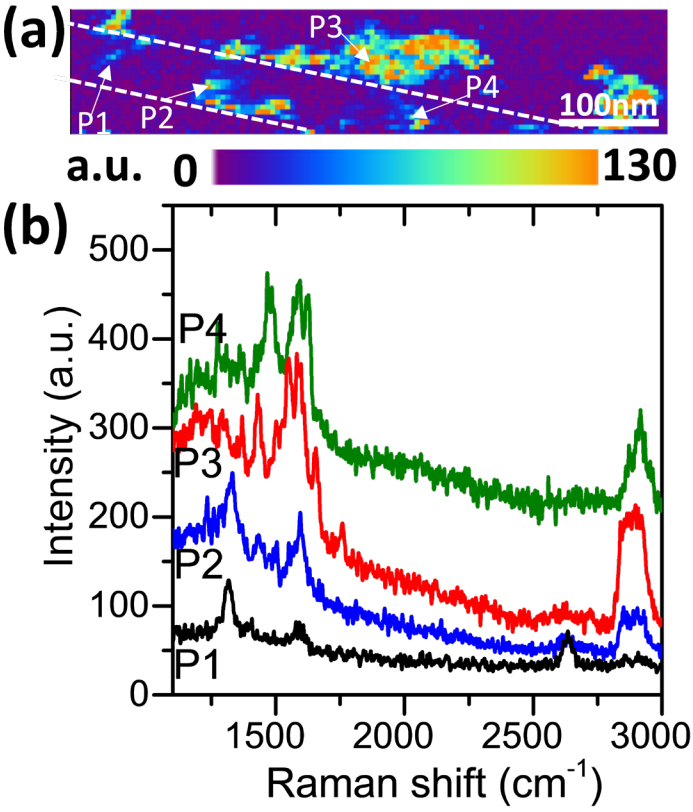

Fig. 4. (a) TERS intensity image of the C-CH_3 band at ~2900 cm^{-1}. (b) Four TERS spectra collected at marked positions P1-P4 in (a).

Conclusion and perspectives

This application note shows how TERS imaging can reveal the presence and the location of defects or contamination induced upon nanopatterning of graphene using EBL. The spatial resolution achieved by TERS imaging of the EBL-fabricated GNRs of a width of ~60 nm is better than 5 nm. Damage along the GNR edge as a result of electron bombardment is observed under the form of amorphous carbon with a thin width (5-10 nm). Organic contaminants originating from PMMA residues can be seen within the GNR or attached to the edge. Such degradation (amorphous carbon or adsorbates) can not be solely visualized by the AFM topography or phase imaging, which makes TERS a powerful tool for characterizing patterned graphene to develop graphene based nano-devices.

Acknowledgments

Weitao Su from Hangzhou Dianzi University and Naresh Kumar from ETH Zurich are thanked for insightful scientific discussions regarding data analysis and interpretation of results.

References

1. P. Avouris, Graphene: Electronic and Photonic Properties and Devices, Nano Lett., 10, 11, 4285–4294 (2010).
2. K. S. Novoselov, A.K. h Geim, S. K. Morozov, D. Jiang, Y. Zhang, S. V. Dubonos, I. V.; Grigorieva, A. A. Firsov, Electric Field Effect in Atomically Thin Carbon Films, Science, 306, 666-669 (2004).
3. Wang, R., Ren, XG., Yan, Z. et al. Graphene based functional devices: A short review. Front. Phys. 14, 13603 (2019).
4. Jiyu Fan, J.M. Michalik, L. Casado, S. Roddaro, M.R. Ibarra, J.M. De Teresa, Investigation of the influence on graphene by using electron-beam and photo-lithography, Solid State Communications, 151, 21, 1574-1578, (2011).
5. I.-S. Byun, D. Yoon, J. S. Choi, I. Hwang, D. H. Lee, M. J. Lee, T. Kawai, Y.-W. Son, Q. Jia, H. Cheong, B. H Park, Nanoscale Lithography on Monolayer Graphene Using Hydrogenation and Oxidation, ACS Nano, 5, 8, 6417–6424 (2011).
6. B . H. Son, H. S. Kim, H. Jeong, Ji-Yong Park, S. Lee, Y. H. Ahn, Electron beam induced removal of PMMA layer used for graphene transfer, Sci Rep 7, 18058 (2017).
7. A. Bhattarai, A. Krayev, A. Temiryazev, D. Evplov, K. T. Crampton, W. P. Hess, P. Z. El-Khoury, Nano Lett., 18, 6, 4029–4033 (2018).
8. R. Beams, Tip-enhanced Raman scattering of graphene, J. Raman Spectrosc., 49: 157– 167 (2018).
9. N. Kumar, B. Stephanidis, R. Zenobi, A. J. Wain, D. Roy, D., Nanoscale Mapping of Catalytic Activity Using Tip-Enhanced Raman Spectroscopy, Nanoscale, 7, 7133-7137 (2015).
10. J. Stadler, T. Schmid, R. Zenobi, Nanoscale Chemical Imaging of Single-Layer Graphene, Acs Nano, 5, 8442-8448 (2011).
11. A.C. Ferrari, J. C. Meyer, V. Scardaci, C. Casiraghi, M. Lazzeri, F. Mauri, S. Piscanec, D. Jiang, K. S. Novoselov, S. Roth, and A. K. Geim, Raman Spectrum of Graphene and Graphene Layers, Phys. Rev. Lett., 97, 187401- 187405 (2006).
12. W. Su, N. Kumar, N. Dai, D. Roy, Nanoscale Mapping of Intrinsic Defects in Single-Layer Graphene Using Tip-Enhanced Raman Spectroscopy. Chem. Commun., 52, 8227-8230 (2016).
13. K.-D. Park, M. B. Raschke, J. M. Atkin, Y. H. Lee, M. S. Jeong, Probing Bilayer Grain Boundaries in Large-Area Graphene with Tip-Enhanced Raman Spectroscopy, Advanced Materials, 29, 1603601 (2017).
14. W. Su, N. Kumar, A. Krayev, M. Chaigneau, In Situ Topographical Chemical and Electrical Imaging of Carboxyl Graphene Oxide at the Nanoscale. Nature Communications, 9, 2891 (2018).
15. A. Jorio, R. Saito, G. Dresselhaus, M.S. Dresselhaus, Raman Spectroscopy in Graphene Related Systems, Wiley-VCH. https://doi.org/10.1002/9783527632695 (2011).

info.sci@horiba.com
www.horiba.com/scientific

HORIBA Scientific

USA: +1 732 494 8660
UK: +44 (0)1604 542 500
China: +86 (0)21 6289 6060
Taiwan: +886 3 5600606
France: +33 (0)1 69 74 72 00
Italy: +39 06 51 59 22 1
India: +91 (80) 4127 3637
Brazil: +55 (0)11 2923 5400
Germany: +49 (0) 6251 8475 0
Japan: +81(75)313-8121
Singapore: +65 (6) 745-8300
Other: +33 (0)1 69 74 72 00